On Error Probability of Massive IoT Slotted ALOHA System in Finite-Length Regime

Tijana Devaja*, Milica Petkovic*, Chao Wang †, Marko Beko‡§, and Dejan Vukobratović*
*Faculty of Technical Sciences, University of Novi Sad, Serbia
† School of Electronics and Information Engineering, Tongji University, Shanghai, China
‡Instituto de Telecomunicações, Instituto Superior Técnico, Universidade de Lisboa, Lisbon, Portugal
§COPELABS, Universidade Lusófona de Humanidades e Tecnologias, Lisbon, Portugal
Email: tijana.devaja@uns.ac.rs, marko.beko@tecnico.ulisboa.pt, dejanv@uns.ac.rs

***Abstract*—In this paper, we present a novel reliability analysis of massive Internet of Things (IoT) connectivity in cellular networks. In massive IoT networks, IoT devices sporadically and unpredictably send short data packets to nearby base stations (BSs), potentially interfering with other IoT devices with whom they share the uplink channel. Assuming slotted ALOHA random access policy, we investigate the probability that an IoT device transmitting a short data packet is not decoded at the nearest BS under Nakagami fading. We derive error probability expressions combining the tools of finite block-length (FBL) information theory and stochastic geometry. Derived FBL-based results are confirmed by Monte Carlo simulations and further compared with the asymptotic expressions available in the previous studies that are obtained under assumption that a device transmits asymptotically long data packets. Numerical results confirm the accuracy of the obtained expressions and their applicability to the massive IoT system design and performance evaluation under a wide range of system parameters. For example, the matching between the values obtained by numerical integration and approximation results of the FBL error probability is in the range between 97.6-99.4 % for different choices of the parameters.**

***Index Terms*—Stochastic geometry, short-packet communication, slotted ALOHA, Finite Block-Length.**

I. Introduction

Massive Internet of Things (IoT) cellular networks such as Narrowband IoT (NB-IoT), LoRaWAN or SigFox are designed to provide massive connectivity to billions of IoT devices that were, until recently, out of reach of wireless IoT technologies [1]. In massive IoT networks, each device engages in a short-packet uplink transmission under an unpredictable activity pattern. To efficiently accommodate such a sporadic short-packet transmission, variations of Slotted ALOHA (SA) are commonly used as a random access mechanism [2]. When a device accesses an SA-based massive IoT network, its transmission is affected by channel impairments and interference from other randomly scattered active devices, while obeying fundamental limits of short-packet transmission quantified by finite block-length (FBL) information theory [3]. The error probability analysis in short-packet IoT communication scenario rests on two main pillars: the interference analysis in large-scale wireless systems obtained using stochastic geometry [4]–[6], and error probability analysis obtained using FBL information theory [7], [8].

Analysis of uplink transmissions in general cellular networks context of coverage probability using the tools of stochastic geometry is well understood [9]. The underlying assumption in this and many other stochastic geometry-based studies that followed is that an IoT device will be decoded at a given BS subject to the threshold signal-to-interference-and-noise (SINR) criteria, i.e., that the device's instantaneous SINR at the BS is above a predefined threshold value. However, under practical system limitations, the error probability vs SINR behavior does not exhibit a sharp threshold behavior unless, e.g., we assume that the system is operated at the Shannon limit using asymptotically long capacity-achieving codes. This indeed is an implicit assumption in coverage probability studies based on SINR-threshold decoding criteria. However, for practical data packet lengths, the error probability vs SINR behavior departs from sharp SINR-threshold transition which makes the existing coverage probability studies only an approximation of a real-world system performance behavior, especially for IoT connectivity services dominated by short packet communications.

In the context of massive IoT networks that rely on short-packet communications[1] , extension of these results using FBL tools leads to more precise error probability analysis. The need to revise the design methodology for wireless network services relying on short packet communications was initially discussed in [3]. The work in [10] addressed the design of massive IoT networks using stochastic geometry under asymptotic (threshold-based) regime. Extension of massive IoT networks to the FBL case, closest to our goal in this work, appeared in the following recent works [12], [13]. However, their work focuses on achievable rate and capacity analysis and does not explicitly target reliability and derivations of closed-form error probability expressions. We note that a combination of stochastic geometry and FBL analysis is gaining atraction and was adopted in recent studies of error probability meta distribution [14], smart grid communications [15], covert mmWave

[1]Short packet communications refer to communication scenarios characterised by small size and specific requirements of transmitted data packets. Finite block-length information theory provides tools for reliability analysis of finite-length data block transmission protected by error correction coding and decoding procedures in channels with noise, and is particularly relevant in the context of short packet communications.

communications [16], reconfigurable intelligent surface (RIS)-assisted communications [17], downlink ultra-reliable and low-latency communications [18]. These studies are followed by proposals of a transmission schemes that are designed to optimise error rates in the FBL regime [19], [20].

In this paper, we focus on error probability analysis of short-packet communications in massive IoT networks and improve the above research studies in several important directions. Firstly, we refine the existing threshold-based error probability result by explicitly taking into account that a device transmits short data packets. Exploiting the results of FBL information theory, we derive a new approximate albeit accurate FBL error probability expressions and compare them with the classical threshold-based results. Secondly, for the latter asymptotic threshold-based results, we present a novel and exact closed-form expressions of error probability under Nakagami fading, thus improving the existing results in the literature.

The Nakagami-m distribution offers several advantages compared to other fading models. It is a generalized distribution capable of representing various fading environments and demonstrates greater flexibility and accuracy in fitting certain experimental data when compared to distributions like Rayleigh or log-normal [21]. Additionally, it's important to highlight that slotted ALOHA-based random access does not reduce general applicability of our results. This is because widely adopted real-world massive IoT protocols such as NB-IoT and LoRaWAN utilize adapted forms of SA in their network access procedures. Therefore, this underscores the relevance and applicability of our findings.

The contributions of this paper are as follows:

1) We provide new approximate yet accurate error probability expressions of massive IoT networks in the FBL regime.
2) We derive approximated closed-form series representations expression of the error probability in FBL regime which improves upon existing literature that often restricts analysis to Rayleigh fading scenarios.
3) Our asymptotic threshold-based error probability results are exact, thus improving the accuracy of approximate results presented in [10].
4) Our results are developed using different analytical approach, targeting a sufficiently general case for which the probability density function (PDF) of interference can be expressed in the closed form [22], [23]. As a consequence, as compared to the results in [10], [13], our results target derivation of explicit error probability expressions, instead of targeting the average rate and capacity analysis.

Monte–Carlo simulations are used to validate the derived analytical results. Numerical results presented in the paper evaluate the accuracy of the obtained expressions in both asymptotic and FBL regime. A careful investigation of error probability is delivered across the range of system parameters (the density and activity of devices, the density of BSs, and the error-correcting code rates and lengths) aiming to facilitate optimal system design of future massive IoT networks.

The rest of the paper is structured as follows. In Section II, we define the system model and set the main hypothesis. In Section III, we analyze the error probability and channel coding rate based on the FBL regime approach. In Section IV we give the detailed analysis of FBL and asymptotic (threshold-based) error probability. In Section V, we present and discuss the numerical results and, finally, in Section VI, we close the paper with the main conclusions.

II. System and Interference Model

We consider a large-scale massive IoT cellular network that contains a set of BSs whose locations form a stationary Poisson Point Process (PPP) denoted by Φ_b of spatial density λ_b on the $\mathbb{R}^2$ plane. The network connects a set of IoT devices whose locations form a stationary PPP Φ_u of spatial density λ_u on $\mathbb{R}^2$. The devices send data to BSs using the SA protocol where we assume the time is divided into equal-length slots. In each slot, every device is active with probability p independently of activity of other devices in the same slot. All active devices are assumed to be attached to the geographically nearest BS. We are interested in the probability that an active device will be successfully decoded at the nearest BS [10]. The error probability analysis will rely on stochastic geometry as an established approach to evaluate the aggregate interference in large-scale wireless networks.

Assuming normalized unit transmit power and Nakagami fading environment, the received power P at a reference BS at the distance r from a reference device is defined as

$$P = hr^{-\eta}, \tag{1}$$

where $r^{-\eta}$ represents the path-loss attenuation with a path loss exponent η, and h is the fading power channel coefficient. Aggregate interference I at any given point in the network originating from the set of all transmitters is defined as

$$I = \sum_{i \in \Phi_u} P_i = \sum_{i \in \Phi_u} a_i h_i {r_i}^{-\eta}, \tag{2}$$

where r_i is a distance of the device $i \in \Phi_u$ from the reception point, a_i is a Bernoulli random variable with parameter p indicating its activity, and h_i is a realization of its fading power. Instantaneous SINR [11] of a device at the distance r from a reference BS is

$$\gamma = \frac{hr^{-\eta}}{I + \sigma^2} \approx \frac{hr^{-\eta}}{I}, \tag{3}$$

where σ^2 is the background noise power, which is usually negligible compared to the cumulative interference.

1) The PDF of the fading power: We consider Nakagami fading where the fading power H follows

$$f_H(h) = \frac{m^m}{\Gamma(m)} h^{m-1} \exp(-mh), \quad h \in (0, +\infty], \tag{4}$$

and m is the fading parameter. For $m = 1$, we obtain a special case of Rayleigh fading.

2) The PDF of the distance between the device and the nearest BS: In the nearest BS model, the device attaches to the geographically nearest BS. The PDF of the distance R between the device and the nearest BS for a PPP is [10]

$$f_R(r) = 2\pi\lambda_b r \exp(-\lambda_b \pi r^2), \quad r \in (0, +\infty]. \tag{5}$$

3) The PDF of the interference power: In order to determine the closed-form expression of the PDF of aggregate interference I, we start with its Laplace transform (LT) defined as [4]

$$\mathcal{L}_I(s) = \exp\Big(- p\lambda_u \pi \mathbb{E}\big[h^{\frac{2}{\eta}}\big]\Gamma(1-\frac{2}{\eta})s^{\frac{2}{\eta}}\Big), \tag{6}$$

where $\Gamma(z)\int_0^\infty x^{z-1}e^{-x}dx$ is the Gamma function [24, (8.31)] and $\mathbb{E}[\cdot]$ is the expectation operator. For Nakagami distributed fading power, the LT of the interference power equals

$$\mathcal{L}_I(s) = \exp\Big(- p\lambda_u \pi \frac{\Gamma\big(m+\frac{2}{\eta}\big)}{\Gamma(m)m^{\frac{2}{\eta}}}\Gamma(1-\frac{2}{\eta})s^{\frac{2}{\eta}}\Big). \tag{7}$$

Authors in [22] noted that the functional form of LT in (7) belongs to a class of Kohlrausch-Williams-Watts (KWW) functions defined as $\mathcal{L}_I(s;\beta) = e^{-s^\beta}$, with parameter β defined as [23]

$$\mathcal{L}_I(s;\beta) = \int_0^\infty \exp(-sI) f_I(x;\beta)\mathrm{d}I = \exp(-s^\beta). \tag{8}$$

They provided closed-form expressions of the interference power PDF $f_I(x;\beta)$ for rational (fractional) values of β. Since in our derivations we will require closed-form expression of the interference power PDF, we will restrict our attention to fractional β values. In general, the PDF $f_I(x;\beta,t)$ of I is obtained using the scaling property of inverse LT (ILT) $\frac{1}{t^\beta} f_I(\frac{x}{t^{\frac{1}{\beta}}};\beta,t) \Longleftrightarrow \exp(-(t^{\frac{1}{\beta}}s)^\beta) = \exp(-ts^\beta)$ [22].

The ILT of $\mathcal{L}_I(s;\beta)$ is investigated for the values of $\beta = \frac{\beta_1}{\beta_2}$ representing a ratio of two integers β_1 and β_2. For example, setting $\beta_1 = 1$ and $\beta_2 = 2$, the ILT of $\mathcal{L}_I(s;\frac{1}{2})$ leads to the simplest PDF expression, known as Lévy distribution

$$f_I(x) = \frac{t\exp(-\frac{t^2}{4x})}{2\sqrt{\pi}x^{\frac{3}{2}}}, \tag{9}$$

where $t = \pi p\lambda_u \frac{\Gamma\left(m+\frac{2}{\eta}\right)}{\Gamma(m)m^{\frac{2}{\eta}}}\Gamma(1-\frac{2}{\eta})$. In the following analysis, we considered the suburban environment, which corresponds to the known case where value of coefficient $\eta = \frac{2}{\beta} = 4$, leading to

$$t = \pi p\lambda_u \frac{\Gamma\big(m+\frac{1}{2}\big)}{\Gamma(m)m^{\frac{1}{2}}}\Gamma(\frac{1}{2}), \tag{10}$$

However, we note that the subsequent analysis is valid for any rational value of β for which $f_I(x)$ is available in the closed form and that such values of β are sufficient to closely approximate relevant path loss exponent η values [22].

Finally, under the system and interference model described above, our goal is to calculate the error probability that an active IoT device is decoded at the nearest BS.

III. Finite Block-length Regime

In this paper, we consider a more precise massive IoT network model where IoT devices transmit short-length data packets encoded using finite-length error correcting code. Our goal is to derive error probability of decoding a short-length data packet of a single active user by taking into account interference contribution from all other active users in a given slot. To put it in the Shannon model context, we are interested in a communication system design that is capable of reliably transmitting with as large as possible rate $R(n;\epsilon,\gamma)$ of bits per symbol of information, while using a code of length n symbols and achieving error probability below ϵ over the channel of parameter γ. Assuming asymptotically long codes $n \to \infty$ and vanishing error probability $\epsilon \to 0$, and treating interference as Gaussian noise, we know that we can operate at the maximum rate R^* equal to Shannon capacity $R^* = C(\gamma) = \log_2(1+\gamma)$. In other words, for a fixed code rate R, there exists a maximum channel parameter γ_{th} under which communicating at rate R is still reliable. This fact justifies common asymptotic (threshold-based) criteria for evaluating coverage probability in large-scale wireless networks (discussed in Sec. IV.C). Under asymptotic (threshold-based) criteria, the error probability of data packet transmission $\epsilon(\gamma)$ as a function of channel parameter γ is approximated with a step function, i.e., $\epsilon(\gamma) = 1$ if $\gamma < \gamma_{\text{th}}$, otherwise, $\epsilon(\gamma) = 0$. For $R = 0.5$, the asymptotic $\epsilon(\gamma)$ step function with $\gamma_{\text{th}} = 2^R - 1 = 0.4142$ is illustrated in Fig. 1.

The above asymptotic approximation of error probability can be made more precise using FBL information theory. For a code of finite length n and the target error probability ϵ, the maximal achievable code rate $R(n;\epsilon,\gamma)$ can be approximated via normal approximation [7]

$$R(n;\epsilon,\gamma) = C(\gamma) - \sqrt{\frac{V(\gamma)}{n}}Q^{-1}(\epsilon), \tag{11}$$

where $Q^{-1}(\cdot)$ denotes the inverse of $Q(x) = \int_x^\infty \frac{1}{2\pi}e^{-\frac{t^2}{2}}\mathrm{d}t$ (the Gaussian Q-function), $V(\gamma) = \gamma\frac{\gamma+2}{(1+\gamma)^2}\log_2^2(e)$ is channel dispersion, and $C(\gamma) = \log_2(1+\gamma)$ is Shannon capacity. From (11), using FBL normal approximation and treating interference as a noise, we obtain the (block) error probability (i.e., the probability a codeword is not decoded at the receiver) conditioned on the SINR γ as

$$\epsilon(\gamma) = Q\left(\sqrt{\frac{n}{V(\gamma)}}\big(C(\gamma) - R\big)\right). \tag{12}$$

Thus, instead of a step-function form of error probability $\epsilon(\gamma)$, in the following analysis, we apply more precise FBL approximation (12). The FBL normal approximation of error probability for $R = 0.5$ and code lengths $n = \{256, 1024\}$ are illustrated in Fig. 1.

Linear approximation of Q-function: In order to approximately solve intractable FBL-based error probability expressions, we will linearly approximate the Q-function form expression in (12). We use a linearization technique [25] for

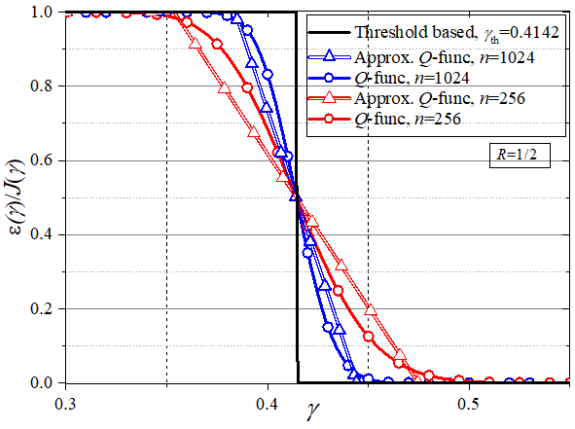

Fig. 1. Comparison between threshold based method $\gamma_{\rm th} = 0.4142$, Q-function in (12) and approximation of a Q-function in (13), for the rate $R = \frac{1}{2}$.

the Q-function in (12), i.e., $Q\Big(\sqrt{\frac{n}{V(\gamma)}}(C(\gamma)-R)\Big) \simeq J(\gamma)$ at point $\gamma = \theta$, to write

$$J(\gamma) = \begin{cases} 1, & \gamma \le \theta - a \\ \frac{1}{2} - \frac{\mu}{\sqrt{2\pi}}(\gamma - \theta), & \theta - a \le \gamma \le \theta + a \\ 0, & \gamma \ge \theta + a \end{cases}, \quad (13)$$

where $a = \sqrt{\frac{\pi}{2\mu^2}}$ for $\theta = 2^R - 1$, $\mu = \sqrt{\frac{n}{2\pi(2^{2R}-1)\log_2^2 e}}$. Linear approximation of FBL-based error probability expression, for $R = 0.5$ and $n = \{256, 1024\}$ is shown in Fig. 1.

IV. Detailed Error Probability Analysis

We now return to the main problem of calculating the error probability that an active IoT user is decoded at the nearest BS. Both FBL and asymptotic (threshold-based) approaches are considered.

A. FBL Error Probability

Based on FBL error probability definition previously given in (12), the final error probability expression for considered uplink communication system can be determined as follows. By conditioning the error probability in (12) over the interference γ, and then further conditioning the interference on fading h and active IoT device-to-nearest BS distance r, we obtain the general FBL error probability expression

$$\begin{aligned} P_e^{\rm fbl} &= \epsilon = \int_{\gamma} \epsilon(\gamma) f_\Gamma(\gamma) {\rm d}\gamma \\ &= \int_r \left(\int_h \left(\int_\gamma \epsilon(\gamma) f_\Gamma(\gamma|h,r) {\rm d}\gamma \right) f_H(h) {\rm d}h \right) f_R(r) {\rm d}r. \end{aligned} \quad (14)$$

In (14), $f_H(h)$ and $f_R(r)$ are defined in (4) and (5), respectively. Furthermore, the conditional SINR distribution $f_\Gamma(\gamma|h,r)$ can be obtained using (3), and evaluated as

$$f_\Gamma(\gamma|h,r) = f_I(\Phi^{-1}(\gamma)) \left| \frac{{\rm d}\Phi^{-1}(\gamma)}{{\rm d}\gamma} \right| = \frac{t \exp(-\frac{t^2\gamma}{4hr^{-4}})}{2\sqrt{\pi h r^{-4}\gamma}}, \quad (15)$$

where the PDF $f_I(x)$ is given in (9). Although (14) can not be derived as a closed-form expression, it can be evaluated by numerical integration or approximated as given below.

B. Approximated FBL Error Probability

Since the error probability in (14) can not be derived as a closed-form expression, the linear approximation of Q-function in (13) is applied. For a short-packet uplink communications, after following derivation in Appendix A, the error probability is tightly approximated as

$$\begin{aligned} P_e^{\rm fbl} \approx & \frac{a_1}{\Gamma(m)\pi} G_{3,3}^{2,3}\Big(z_1 \Big| {}^{1,0,\frac{1}{2}}_{\frac{1}{2},m,0}\Big) + \frac{a_2}{\Gamma(m)\pi} G_{3,3}^{2,3}\Big(z_2 \Big| {}^{1,0,\frac{1}{2}}_{\frac{1}{2},m,0}\Big) \\ & - b_1 z_1 \big(c + d {z_1}^{m-\frac{1}{2}}\big) + b_2 z_2 \big(c + d {z_2}^{m-\frac{1}{2}}\big), \end{aligned} \quad (16)$$

where

$$\begin{aligned} a_1 &= \left(\frac{1}{2} + \frac{\mu\theta}{\sqrt{2\pi}}\right), \quad a_2 = \left(\frac{1}{2} - \frac{\mu\theta}{\sqrt{2\pi}}\right) \\ b_1 &= \frac{\mu(\theta+a)}{\sqrt{2\pi}}, \quad b_2 = \frac{\mu(\theta-a)}{\sqrt{2\pi}}, \\ z_1 &= \frac{t^2(\theta+a)m}{(\lambda_b \pi)^2}, \quad z_2 = \frac{t^2(\theta-a)m}{(\lambda_b \pi)^2}, \\ c &= \frac{\Gamma(m-\frac{1}{2})}{3\sqrt{\pi}\Gamma(m)}, \quad d = \frac{(-1)^m m}{m+1}, \end{aligned} \quad (17)$$

where $G_{p,q}^{m,n}(\cdot|\,\cdot)$ is the Meijer's G-function [26, (9.301)].

Note that argument of the Meijer's G-functions in (16) is very small for practical system parameters ($\frac{t^2(\theta \pm a)m}{(\lambda_b \pi)^2} \to 0$). Series representations of Meijer's G-function when its argument tends to zero can be applied by utilizing [26, (07.34.06.0001.01)], which lead to the simple closed-form expression of the error probability

$$\begin{aligned} P_{e,\rm app}^{\rm fbl} \approx & a_1 \big(3c {z_1}^{\frac{1}{2}} + (-1)^m z_1^m\big) + a_2 \big(3c z_2^{\frac{1}{2}} + (-1)^m z_2^m\big) \\ & - b_1 z_1 \big(c + d {z_1}^{m-\frac{1}{2}}\big) + b_2 z_2 \big(c + d {z_2}^{m-\frac{1}{2}}\big). \end{aligned} \quad (18)$$

C. Asymptotic (threshold-based) Error Probability

In order to better understand the novel FBL approximation (16), we step back and rederive the classical asymptotic threshold-based error probability analysis. Note that we do it for a more general Nakagami fading, while providing exact closed-form expressions, unlike approximate expressions presented in [10], [13]. The threshold-based decoding criteria assumes that an error event occurs if the SINR γ, defined in (3), is below a predefined threshold $\gamma_{\rm th}$. We obtain the SINR threshold value $\gamma_{\rm th}$ for a given R and $n \to \infty$ as discussed in Sec. III [10].

Formally, the asymptotic error probability P_e can be expressed as

$$P_e = \mathbb{P}[\gamma \le \gamma_{\rm th}] = \mathbb{P}\Big[\frac{hr^{-\eta}}{I} \le \gamma_{\rm th}\Big] = 1 - \mathbb{P}[I \le \frac{hr^{-\eta}}{\gamma_{\rm th}}], \quad (19)$$

where $\gamma_{\rm th}$ represents the SINR threshold.

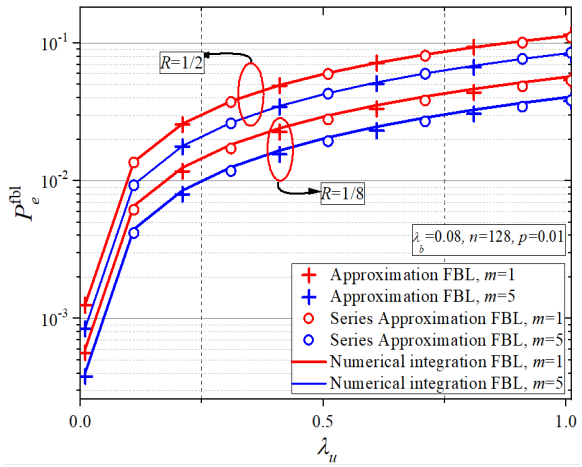

Fig. 2. Comparison between FBL error probability P_e^{fbl} obtained by numerical integration (14), approximation (16) and series approximation (18) for different R, m and fixed values of $\lambda_b = 0.04$, $n = 128$, and $p = 0.01$.

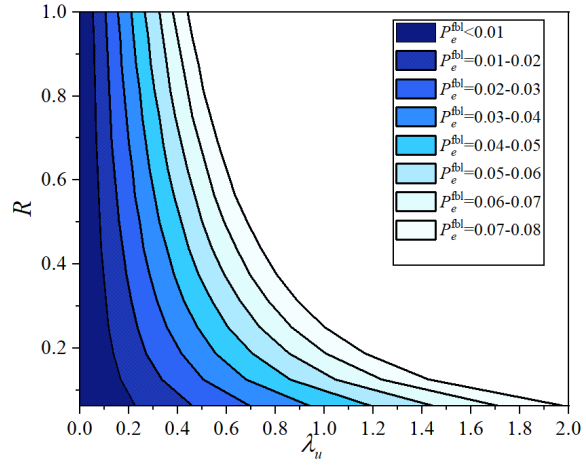

Fig. 3. Density of users λ_u vs. different coding rates R for error probability in FBL regime for $\mu = 1$.

The probability that a device, affected by Nakagami fading, is not decoded at the nearest BS under the threshold-based criterion can be determined as

$$P_e = 1 - \int_0^\infty \left(\int_0^\infty \left(\int_0^{\frac{hr^{-\eta}}{\gamma_{\text{th}}}} f_I(x)\mathrm{d}x \right) f_H(h)\mathrm{d}h \right) f_R(r)\mathrm{d}r, \quad (20)$$

where $f_H(h), f_R(r)$ and $f_I(x)$ are defined in (4), (5) and (9) respectively.

For the suburban environment we present a novel closed-form expression for the asymptotic error probability as

$$P_e = 1 - \frac{1}{\Gamma(m)\pi} G_{3,3}^{3,2}\left(\frac{t^2 \gamma_{\text{th}} m}{(\lambda_b \pi)^2} \,\middle|\, \begin{matrix} 0, \frac{1}{2}, 1 \\ \frac{1}{2}, m, 0 \end{matrix} \right). \quad (21)$$

Analysis is valid for any rational value of β for which $f_I(x)$ is available in the closed form. Note that this result is a closed-form solution, completing the approximate analysis in [10]. Complete derivation is shown in Appendix B.

Approximation: After applying [26, (07.34.06.0001.01)] to transform the Meijer's G-function into a series form when its argument tends to zero, and after removing the higher-order terms of the series representation, the approximation of the threshold-based error probability for large values of λ_b and/or low values of λ_u or p is derived as

$$P_e \approx 3cz^{\frac{1}{2}} - (-1)^m m z^m, \quad (22)$$

where $z = \frac{t^2 \gamma_{\text{th}} m}{(\lambda_b \pi)^2}$ and c is previously defined in (17).

V. Numerical and Simulation Results

In this section, using the analysis presented in Sec. IV, we consider the design and performance evaluation of the massive IoT network model.

A. Numerical results

Fig. 2 depicts comparison between the results of the FBL error probability P_e^{fbl} obtained by numerical integration in (14), approximation defined in (16) and series approximation defined in (18). Increasing the code rate R leads to deterioration of error probability. For lower values of the Nakagami parameter m, fading is more severe and worsening of the system performance is noticed. If we observe the difference between the numerical integration and both approximation curves, we note that for the higher code rates, the approximation becomes more accurate. This follows from linear approximation of Q-function, where as the code rates R increases, one can easily verify the improved accuracy of linear Q-function approximation. The matching between exact values obtained by numerical integration and approximation results of the FBL error probability is in the range between 97.6-99.4% for different choices of the parameters R, m and fixed values of λ_b = 0.04, n = 128, and p = 0.01.

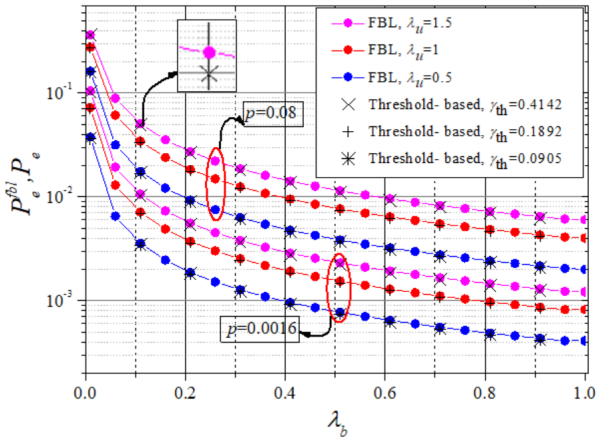

Fig. 4. Error probability vs. λ_b for asymptotic method P_e where $m = 1$, $R = 1/8$ and $n \to \infty$, and FBL method P_e^{fbl} with $R = 1/8$ and $n = 128$.

Using the FBL error probability P_e^{fbl} approximation, one can easily explore the system performance across the range of code rates R and user densities λ_u as shown in Fig. 3. From the figure, for a desired P_e^{fbl}, a range of (λ_u, R) pairs

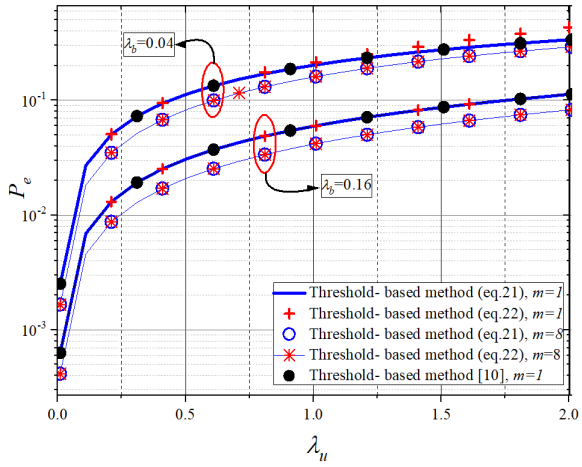

Fig. 5. Error probability P_e vs. density of users λ_u for asymptotic threshold-based method approximation (21) and series approximation (22). Different λ_b and m are used, activation rate is $p = 0.01$ and threshold is $\gamma_{\text{th}} = 0.4142$.

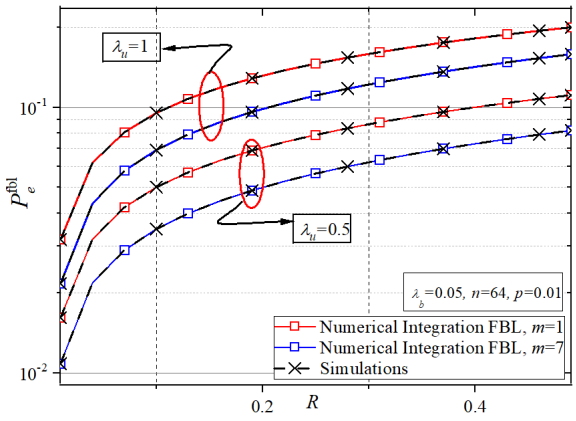

Fig. 6. Comparison between FBL error probability P_e^{fbl} obtained by numerical integration (14) and simulations for different density of users λ_u, and Nakagami parameter m. Values are fixed for density of BS $\lambda_b = 0.08$, code length $n = 64$, and activation probability $p = 0.01$.

provide a solution. In other words, one can counterbalance the increase in the system load λ_u with appropriate control of the code rate R while achieving a desired reliability level.

Fig. 4 presents the error probability dependence on the BSs spatial density λ_b for both asymptotic (P_e) and FBL (P_e^{fbl}) method. For the former, we assume capacity-achieving error-correcting code of rate $R = \frac{1}{8}$ and length $n \to \infty$, while for the latter, we assume normal approximation achieving code of the same rate and $n = 128$ (FBL). In order to mitigate transmission latency and yield high reliability, codeword lengths of the order of $n \approx 100$ symbols are most commonly used in simulation studies [3], [7]. The error probability is presented for several values of users densities λ_u and activation probabilities p. Increasing both the activation probability p and the density of users λ_u, the error probability deteriorates, due to the increase in aggregate interference.

Fig. 5 shows the error probability P_e a device experiences at its nearest BS for two values of BS density ($\lambda_b = 0.04$ and $\lambda_b = 0.16$), under varying density of users λ_u, where a device activity rate is fixed to $p = 0.01$. The results of closed-form expression (21) match approximated series representation (22), validating the analysis from Sec. IV.C. The graph demonstrates the following trends: i) increasing the density of BS λ_b results in the decrease of the error probability due to the shift of $f_R(r)$ towards lower distances, ii) error probability increases with higher λ_u due to increased interference, and iii) increasing the Nakagami parameter m results in decrease in error probability. Additionally, approximate error probability under Rayleigh fading results derived in [10] are also presented in Fig. 5, which are overlapping with our results for $m = 1$ (the special case of Nakagami fading scenario).

B. Numerical vs Simulation Results Analysis

We develop a simulator in which devices and BS are deployed according to a PPP. To verify our results, the probability of error obtained analytically has been compared to their respective Monte Carlo simulation results with 3000 trials. Comparison between FBL error probability (P_e^{fbl}) obtained by numerical integration and simulations is depicted in Fig. 6 for different values of Nakagami parameter m and density of users λ_u. The graph shows almost perfect matching between simulation and analytical results, and by increasing the density of users λ_u, and code rate R the error probability deteriorates.

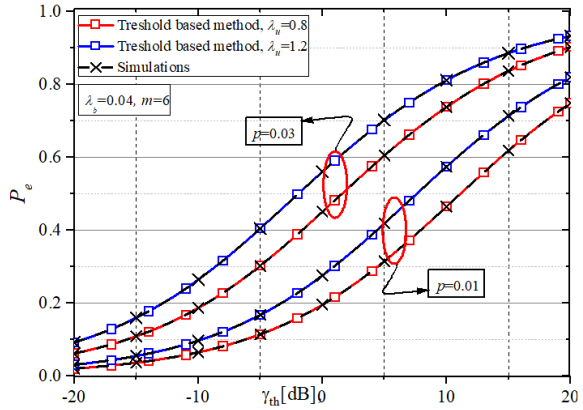

Fig. 7. Error probability P_e vs. threshold γ_{th}, for asymptotic threshold-based method approximation (22). Different density of users λ_u and activation rates p are used, density of BS is $\lambda_b = 0.04$ and Nakagami coefficient $m = 6$.

In order to verify our results, the probability of error for the threshold based method has been compared to their respective Monte Carlo simulation results with 3000 trials. Fig. 7 shows the error probability P_e a device experiences at its nearest BS versus threshold γ_{th} in dB scale. For this network configuration, as expected, the probability of error gets higher with the increase of threshold level. The error probability is shown for several values of users densities λ_u and activation probabilities p. Increasing both the activation probability p and the density of users λ_u, the error probability deteriorates, due to the increase in aggregate interference.

VI. Conclusion

In this work, we analysed expressions for error probability an IoT device experiences at the nearest BS under Nakagami fading and interference from PPP-distributed interferers. We focus on the finite-block length model, where an approximate analysis based on FBL information theory is derived. We presented the detailed derivation and investigation of numerical accuracy of both FBL and asymptotic expressions, and demonstrated their usage in the design of massive IoT networks. In the future work, we plan to extend our results to various fading and shadowing distributions and random access models beyond the conventional but widespread SA protocol.

Acknowledgment

This work has received funding from the Horizon 2020 research and innovation staff exchange grant agreement No 101086387, the 2021-2023 China-Serbia Inter- Governmental S&T Cooperation Project (No. 6), the Science Fund of the Republic of Serbia, grant number 6707, REmote WAter quality monitoRing anD IntelliGence – REWARDING and by the Secretariat for Higher Education and Scientific Research of the Autonomous Province of Vojvodina through the project "Visible light technologies for indoor sensing, localization and communication in smart buildings" (142-451-2686/2021).

Appendix A

Approximation of $Q(\cdot)$ function at point $\theta = 2^R - 1$ based on a linearization technique was shown in (13). After substituting (13) into (14), the approximation of the error probability is defined as

$$\begin{aligned} P_e^{\text{fbl}} &\approx \int_0^\infty\int_0^\infty\int_0^{\theta-a} f_\Gamma(\gamma|h,r) f_H(h) f_R(r) \mathrm{d}\gamma \mathrm{d}h \mathrm{d}r \\ &+ \int_0^\infty\int_0^\infty\int_{\theta-a}^{\theta+a} (\frac{1}{2} - \frac{\mu(\gamma-\theta)}{\sqrt{2\pi}}) f_\Gamma(\gamma|h,r) f_H(h) f_R(r) \mathrm{d}\gamma \mathrm{d}h \mathrm{d}r \\ &= I_1 + I_2, \end{aligned} \tag{23}$$

where μ and a are previously defined in Sec. III, and triple integrals in (23) are defined as

$$I_1 = \int_0^\infty\int_0^\infty\int_0^{\theta-a} f_\Gamma(\gamma|h,r) f_H(h) f_R(r) \mathrm{d}\gamma \mathrm{d}h \mathrm{d}r, \tag{24}$$

and

$$I_2 = \int_0^\infty\int_0^\infty\int_{\theta-a}^{\theta+a} (\frac{1}{2} - \frac{\mu(\gamma-\theta)}{\sqrt{2\pi}}) f_\Gamma(\gamma|h,r) f_H(h) f_R(r) \mathrm{d}\gamma \mathrm{d}h \mathrm{d}r. \tag{25}$$

After substituting (4), (5) and (15) into (24), the first triple integral in (24) is re-written as

$$\begin{aligned} I_1 = \int_0^\infty \Bigg(\int_0^\infty \Bigg(\int_0^{\theta-a} \frac{t e^{-\frac{t^2\gamma}{4hr^{-4}}}}{2\sqrt{\pi h r^{-4}}} \gamma^{-\frac{1}{2}} \mathrm{d}\gamma \Bigg) \\ \times \frac{m^m}{\Gamma(m)} h^{m-1} e^{-mh} \mathrm{d}h \Bigg) 2\pi\lambda_b r e^{-\lambda_b \pi r^2} \mathrm{d}r \Bigg) \end{aligned} \tag{26}$$

After solving the inner integral in (26) over γ with the help of [24, (8.251)] as $\int_0^{\theta-a} \frac{t e^{-\frac{t^2\gamma}{4hr^{-4}}}}{2\sqrt{\pi h r^{-4}}} \gamma^{-\frac{1}{2}} \mathrm{d}\gamma = (\frac{t\sqrt{\theta-a}}{2\sqrt{hr^{-4}}})$, the integral I_1 is now rewritten as

$$\begin{aligned} I_1 = \frac{m^m}{\Gamma(m)} \int_0^\infty \Bigg(\int_0^\infty h^{m-1} e^{-mh} \Bigg(\frac{t\sqrt{\theta-a}}{2\sqrt{hr^{-4}}} \Bigg) \mathrm{d}h \Bigg) \\ \times 2\pi\lambda_b r e^{-\lambda_b \pi r^2} \mathrm{d}r. \end{aligned} \tag{27}$$

After representing the exponential function in terms of Meijer's *G*-functions by using [26, (01.03.26.0004.01)] as $e^{-mh} = G_{0,1}^{1,0}\big(mh \,\big|\, \begin{smallmatrix} - \\ 0 \end{smallmatrix}\big)$, and the error function function by using [26, (06.25.26.0006.01) and (07.34.21.0011.01)] as $\mathrm{erf}(\frac{t\sqrt{\theta-a}}{2\sqrt{hr^{-4}}}) = \frac{1}{\sqrt{\pi}} G_{2,1}^{1,1}\Big(\frac{4hr^{-4}}{t^2(\theta-a)} \,\Big|\, \begin{smallmatrix} \frac{1}{2}, 1 \\ 0 \end{smallmatrix}\Big)$, respectively, the inner integral over h is solved with the help of [26, (07.34.21.0011.01)]. Afterwards, the error probability in (27) can be written as

$$I_1 = \frac{2\lambda_b\sqrt{\pi}}{\Gamma(m)} \int_0^\infty r e^{-\lambda_b\pi r^2} G_{3,1}^{1,2}\Bigg(\frac{4r^{-4}}{t^2(\theta-a)m} \,\Bigg|\, \begin{smallmatrix} \frac{1}{2}, 1-m, 1 \\ 0 \end{smallmatrix}\Bigg) \mathrm{d}r. \tag{28}$$

Following the exponential function presentation in terms of Meijer's *G*-functions by [26, (01.03.26.0004.01)] as $e^{-\lambda_b\pi r^2} = G_{0,1}^{1,0}\big(\lambda_b\pi r^2 \,\big|\, \begin{smallmatrix} - \\ 0 \end{smallmatrix}\big)$ and the change of variables $r^2 = x$, the integral I_1 is finally solved with the help of [26, (07.34.16.0002.01) and (07.34.21.0013.01)] as

$$\begin{aligned} I_1 &= \frac{\lambda_b\sqrt{\pi}}{\Gamma(m)} \int_0^\infty G_{0,1}^{1,0}\big(\lambda_b\pi x \,\big|\, \begin{smallmatrix} - \\ 0 \end{smallmatrix}\big) G_{1,3}^{2,1}\Bigg(\frac{t^2(\theta-a)mx^2}{4} \,\Bigg|\, \begin{smallmatrix} 1 \\ \frac{1}{2}, m, 0 \end{smallmatrix}\Bigg) \mathrm{d}x \\ &= \frac{1}{\Gamma(m)\pi} G_{3,3}^{2,3}\Bigg(\frac{t^2(\theta-a)m}{(\lambda_b\pi)^2} \,\Bigg|\, \begin{smallmatrix} 1, 0, \frac{1}{2} \\ \frac{1}{2}, m, 0 \end{smallmatrix}\Bigg). \end{aligned} \tag{29}$$

Next, we will deal with the second triple integral I_2 in (25), which can be presented as a sum of three integrals as

$$\begin{aligned} I_2 &= \int_0^\infty\int_0^\infty\int_{\theta-a}^{\theta+a} (\frac{1}{2} - \frac{\mu(\gamma-\theta)}{\sqrt{2\pi}}) f_\Gamma(\gamma|h,r) f_H(h) f_R(r) \mathrm{d}\gamma \mathrm{d}h \mathrm{d}r \\ &= I_{21} - I_{22} + I_{23}, \end{aligned} \tag{30}$$

where

$$I_{21} = \int_0^\infty\int_0^\infty\int_{\theta-a}^{\theta+a} \frac{1}{2} f_\Gamma(\gamma|h,r) f_H(h) f_R(r) \mathrm{d}\gamma \mathrm{d}h \mathrm{d}r, \tag{31}$$

$$I_{22} = \int_0^\infty\int_0^\infty\int_{\theta-a}^{\theta+a} \frac{\mu\gamma}{\sqrt{2\pi}} f_\Gamma(\gamma|h,r) f_H(h) f_R(r) \mathrm{d}\gamma \mathrm{d}h \mathrm{d}r, \tag{32}$$

$$I_{23} = \int_0^\infty\int_0^\infty\int_{\theta-a}^{\theta+a} \frac{\mu\theta}{\sqrt{2\pi}} f_\Gamma(\gamma|h,r) f_H(h) f_R(r) \mathrm{d}\gamma \mathrm{d}h \mathrm{d}r. \tag{33}$$

After substituting (4), (5) and (15) into (31), the integral I_{21} is re-written as

$$\begin{aligned} I_{21} = \int_0^\infty \Bigg(\int_0^\infty \Bigg(\int_{\theta-a}^{\theta+a} \frac{t e^{-\frac{t^2\gamma}{4hr^{-4}}}}{4\sqrt{\pi h r^{-4}}} \gamma^{-\frac{1}{2}} \mathrm{d}\gamma \Bigg) \\ \times \frac{m^m}{\Gamma(m)} h^{m-1} e^{-mh} \mathrm{d}h \Bigg) 2\pi\lambda_b r e^{-\lambda_b \pi r^2} \mathrm{d}r \Bigg), \end{aligned} \tag{34}$$

The inner integral in (34) over γ is solved by [24, (8.251)] as $\int_{\theta-a}^{\theta+a} \frac{te^{-\frac{t^2\gamma}{4hr^{-4}}}}{4\sqrt{\pi hr^{-4}}}\gamma^{-\frac{1}{2}}\mathrm{d}\gamma = \frac{1}{2}(\frac{t\sqrt{\theta+a}}{2\sqrt{hr^{-4}}}) - \frac{1}{2}(\frac{t\sqrt{\theta-a}}{2\sqrt{hr^{-4}}})$, leading to the new form of integral I_{21}

$$I_{21} = \int_0^\infty \Bigg(\int_0^\infty \Bigg(\frac{1}{2}(\frac{t\sqrt{\theta+a}}{2\sqrt{hr^{-4}}}) - \frac{1}{2}(\frac{t\sqrt{\theta-a}}{2\sqrt{hr^{-4}}}) \Bigg) \times \frac{m^m}{\Gamma(m)} h^{m-1} e^{-mh} \mathrm{d}h \Bigg) 2\pi\lambda_b r e^{-\lambda_b \pi r^2} \mathrm{d}r \Bigg). \tag{35}$$

Since both integrals over h and r in (35) are similar as the corresponding ones in (27), after following the same steps early described (derivation from (27) to (29)), the final expression of I_{21} is determined as

$$I_{21} = \frac{1}{2\Gamma(m)\pi} \Bigg(G_{3,3}^{2,3}\Bigg(\frac{t^2(\theta+a)m}{(\lambda_b\pi)^2} \,\Bigg|\, \begin{smallmatrix} 1,0,\frac{1}{2} \\ \frac{1}{2},m,0 \end{smallmatrix} \Bigg) - G_{3,3}^{2,3}\Bigg(\frac{t^2(\theta-a)m}{(\lambda_b\pi)^2} \,\Bigg|\, \begin{smallmatrix} 1,0,\frac{1}{2} \\ \frac{1}{2},m,0 \end{smallmatrix} \Bigg) \Bigg). \tag{36}$$

After substituting (4), (5) and (15) into (33), integral I_{23} is re-written and solved by following the same procedure as in derivation of I_{21}

$$\begin{aligned} I_{23} &= \int_0^\infty \Bigg(\int_0^\infty \Bigg(\int_{\theta-a}^{\theta+a} \frac{\mu\theta}{\sqrt{2\pi}} \frac{te^{-\frac{t^2\gamma}{4hr^{-4}}}}{2\sqrt{\pi hr^{-4}}} \gamma^{-\frac{1}{2}} \mathrm{d}\gamma \Bigg) \times \frac{m^m}{\Gamma(m)} h^{m-1} e^{-mh} \mathrm{d}h \Bigg) 2\pi\lambda_b r e^{-\lambda_b\pi r^2} \mathrm{d}r \Bigg) \\ &= \frac{\mu\theta}{\Gamma(m)\pi\sqrt{2\pi}} \Bigg(G_{3,3}^{2,3}\Bigg(\frac{t^2(\theta+a)m}{(\lambda_b\pi)^2} \,\Bigg|\, \begin{smallmatrix} 1,0,\frac{1}{2} \\ \frac{1}{2},m,0 \end{smallmatrix} \Bigg) - G_{3,3}^{2,3}\Bigg(\frac{t^2(\theta-a)m}{(\lambda_b\pi)^2} \,\Bigg|\, \begin{smallmatrix} 1,0,\frac{1}{2} \\ \frac{1}{2},m,0 \end{smallmatrix} \Bigg) \Bigg). \end{aligned} \tag{37}$$

After substituting (4), (5) and (15) into (32), the integral I_{22} is re-written as

$$I_{22} = \int_0^\infty \Bigg(\int_0^\infty \Bigg(\int_{\theta-a}^{\theta+a} \frac{\mu t e^{-\frac{t^2\gamma}{4hr^{-4}}}}{2\pi\sqrt{2hr^{-4}}} \gamma^{\frac{1}{2}} \mathrm{d}\gamma \Bigg) \times \frac{m^m}{\Gamma(m)} h^{m-1} e^{-mh} \mathrm{d}h \Bigg) 2\pi\lambda_b r e^{-\lambda_b\pi r^2} \mathrm{d}r \Bigg), \tag{38}$$

The inner integral in (38) over γ is solved as

$$I_{22} = \int_0^\infty \Bigg(\int_0^\infty \frac{\mu t}{2\pi\sqrt{2hr^{-\eta}}} \frac{m^m}{\Gamma(m)} h^{m-1} e^{-mh} \mathrm{d}h \Bigg) \times \Bigg((\theta+a)^{\frac{3}{2}} E_{-\frac{1}{2}}\big(\frac{t^2}{4hr^{-\eta}}(\theta+a) \big) - (\theta-a)^{\frac{3}{2}} E_{-\frac{1}{2}}\big(\frac{t^2}{4hr^{-\eta}}(\theta-a) \big) \Bigg) f_R(r)\mathrm{d}r \Bigg), \tag{39}$$

where $E_v(z)$ represents exponential integral defined in [26, (06.34.07.0001.01)]. Exponential function is represented in terms of Meijer's G-function by [26, (01.03.26.0004.01)] as $e^{-h} = G_{0,1}^{1,0}\big(h \,\big|\, \begin{smallmatrix} - \\ 0 \end{smallmatrix}\big)$, while [26, (06.34.26.0005.01) and (07.34.16.0002.01)] can be used to transform exponential integral function into Meijer's G-function. Integral over h in (39) can be solved using [26, (07.34.21.0011.01) and (07.34.16.0002.01)] as

$$\begin{aligned} I_{22} = \int_0^\infty & \frac{\mu t\sqrt{m}}{2\sqrt{2}\pi\Gamma(m)} r^2 2\pi\lambda_b r e^{-\lambda_b\pi r^2} \\ & \times \Bigg((\theta+a)^{\frac{3}{2}} G_{1,3}^{3,0}\Bigg(\frac{t^2(\theta+a)mr^4}{4} \,\Bigg|\, \begin{smallmatrix} -\frac{1}{2} \\ -\frac{3}{2},0,m-\frac{1}{2} \end{smallmatrix} \Bigg) \\ & - (\theta-a)^{\frac{3}{2}} G_{1,3}^{3,0}\Bigg(\frac{t^2(\theta-a)mr^4}{4} \,\Bigg|\, \begin{smallmatrix} -\frac{1}{2} \\ -\frac{3}{2},0,m-\frac{1}{2} \end{smallmatrix} \Bigg) \Bigg) \mathrm{d}r. \end{aligned} \tag{40}$$

Next, exponential function in (40) is represented in terms of Meijer's G-function by [26, (01.03.26.0004.01)] as $e^{-\lambda_b\pi r^2} = G_{0,1}^{1,0}\big(\lambda_b\pi r^2 \,\big|\, \begin{smallmatrix} - \\ 0 \end{smallmatrix}\big)$. Integral in (40) does not converge over the specified interval $\{0,\infty\}$, thus we use series representation of Meijer's G-function [26, (07.34.06.0001.01)] in order to have high precision approximation. Afterwards, integral in (40) is easily solved as

$$I_{22} = -b_1 z_1 \big(c + dz_1{}^{m-\frac{1}{2}}\big) + b_2 z_2 \big(c + dz_2{}^{m-\frac{1}{2}}\big), \tag{41}$$

After substituting (36), (37) and (41) into (30), integral I_2 is approximated as

$$\begin{aligned} I_2 = & \frac{a_1}{\Gamma(m)\pi} G_{3,3}^{2,3}\Big(z_1 \,\Big|\, \begin{smallmatrix} 1,0,\frac{1}{2} \\ \frac{1}{2},m,0 \end{smallmatrix} \Big) - \frac{a_1}{\Gamma(m)\pi} G_{3,3}^{2,3}\Big(z_2 \,\Big|\, \begin{smallmatrix} 1,0,\frac{1}{2} \\ \frac{1}{2},m,0 \end{smallmatrix} \Big) \\ & + b_1 z_1 \big(c + dz_1{}^{m-\frac{1}{2}}\big) - b_2 z_2 \big(c + dz_2{}^{m-\frac{1}{2}}\big) \end{aligned} \tag{42}$$

where $a_1, a_2, b_1, b_2, c, z_1, z_2$ are defined in (17).

After substituting (29) and (42), the final approximate FBL error probability is derived and given by (16). The deviation from the exact values of error probability will be determined based on the expression given in (14), which will be calculated by numerical integration.

APPENDIX B

In order to derive the threshold-based error probability in (20), the first step is to substitute the interference PDF $f_I(x)$ given by (9) in (20)

$$P_e = 1 - \int_0^\infty \Bigg(\int_0^\infty \Bigg(\int_0^{\frac{hr^{-4}}{\gamma_{\mathrm{th}}}} \frac{te^{-\frac{t^2}{4x}}}{2\sqrt{\pi}x^{\frac{3}{2}}} \mathrm{d}x \Bigg) f_H(h)\mathrm{d}h \Bigg) f_R(r)\mathrm{d}r. \tag{43}$$

The inner integral over x is solved by [24, (3.361.1)] as $\int_0^{\frac{hr^{-4}}{\gamma_{\mathrm{th}}}} \frac{te^{-\frac{t^2}{4x}}}{2\sqrt{\pi}x^{\frac{3}{2}}}\mathrm{d}x = \mathrm{erfc}\Bigg(\frac{t}{2}\sqrt{\frac{\gamma_{\mathrm{th}}}{hr^{-4}}} \Bigg)$, where $\mathrm{erfc}(\cdot)$ is the complementary error function defined in [24, (8.250.4)]. After substituting solution of the integral over x in (43), and the replacement of the PDF of the fading power given by (4), the error probability in (43) is rewritten as

$$P_e = 1 - \int_0^\infty \Bigg(\int_0^\infty \mathrm{erfc}\Bigg(\frac{t}{2}\sqrt{\frac{\gamma_{\mathrm{th}}}{hr^{-4}}} \Bigg) \frac{m^m}{\Gamma(m)} h^{m-1} e^{-mh} \mathrm{d}h \Bigg) f_R(r)\mathrm{d}r. \tag{44}$$

Exponential function is represented in terms of Meijer's G-function [26, (01.03.26.0004.01)] as $e^{-h} = G_{0,1}^{1,0}\big(h \,\big|\, \begin{smallmatrix} - \\ 0 \end{smallmatrix}\big)$, while [26, (06.27.26.0006.01) and (07.34.16.0002.01)]

can be used for the complementary error function as $\operatorname{erfc}\left(\frac{t}{2}\sqrt{\frac{\gamma_{\rm th}}{hr^{-4}}}\right) = \frac{1}{\sqrt{\pi}} G_{2,1}^{0,2}\left(\frac{4r^{-4}h}{t^2\gamma_{\rm th}} \middle| \begin{smallmatrix} 1, \frac{1}{2} \\ 0 \end{smallmatrix}\right)$. Afterwards, the error probability in (44) can be written as

$$P_e = 1 - \frac{m^m}{\sqrt{\pi}\Gamma(m)} \int_0^\infty \left(\int_0^\infty h^{m-1} G_{0,1}^{1,0}\left(mh \,\middle|\, \begin{smallmatrix} - \\ 0 \end{smallmatrix}\right) \times G_{2,1}^{0,2}\left(\frac{4r^{-4}}{t^2\gamma_{\rm th}} h \middle| \begin{smallmatrix} 1, \frac{1}{2} \\ 0 \end{smallmatrix}\right) dh \right) f_R(r) \mathrm{d}r. \tag{45}$$

Integral over h in (45) is solved by [26, (07.34.21.0011.01)] as

$$\int_0^\infty h^{m-1} G_{0,1}^{1,0}\left(mh \middle| \begin{smallmatrix} - \\ 0 \end{smallmatrix}\right) G_{2,1}^{0,2}\left(\frac{4r^{-4}h}{t^2\gamma_{\rm th}} \middle| \begin{smallmatrix} 1, \frac{1}{2} \\ 0 \end{smallmatrix}\right) \mathrm{d}h = m^{-m} G_{3,1}^{0,3}\left(\frac{4r^{-4}}{t^2\gamma_{\rm th} m} \middle| \begin{smallmatrix} 1, \frac{1}{2}, 1-m \\ 0 \end{smallmatrix}\right). \tag{46}$$

After substituting (46) and $f_R(r)$ given by (5) into (45), the error probability is rewritten as

$$P_e = 1 - \frac{2\pi\lambda_b}{\sqrt{\pi}\Gamma(m)} \times \int_0^\infty r e^{-\lambda_b \pi r^2} G_{3,1}^{0,3}\left(\frac{4r^{-4}}{t^2\gamma_{\rm th} m} \middle| \begin{smallmatrix} 1, \frac{1}{2}, 1-m \\ 0 \end{smallmatrix}\right) \mathrm{d}r. \tag{47}$$

After applying the change of variables $r^2 = u$, [26, (07.34.16.0002.01)] is used to perform transformation of Meijer's G-function as

$$G_{3,1}^{0,3}\left(\frac{4u^{-2}}{t^2\gamma_{\rm th} m} \middle| \begin{smallmatrix} 1, \frac{1}{2}, 1-m \\ 0 \end{smallmatrix}\right) = G_{1,3}^{3,0}\left(\frac{t^2\gamma_{\rm th} m}{4} u^2 \middle| \begin{smallmatrix} 1 \\ 0, \frac{1}{2}, m \end{smallmatrix}\right), \tag{48}$$

while the the exponential function is represented in terms of Meijer's G-function as $e^{-\lambda_b \pi u} = G_{0,1}^{1,0}\left(\lambda_b \pi u \,\middle|\, \begin{smallmatrix} - \\ 0 \end{smallmatrix}\right)$ based on [26, (01.03.26.0004.01)]. Finally, the error probability expression is re-written as

$$P_e = 1 - \frac{\pi\lambda_b}{\sqrt{\pi}\Gamma(m)} \times \int_0^\infty G_{0,1}^{1,0}\left(\lambda_b \pi u \,\middle|\, \begin{smallmatrix} - \\ 0 \end{smallmatrix}\right) G_{1,3}^{3,0}\left(\frac{t^2\gamma_{\rm th} m}{4} u^2 \middle| \begin{smallmatrix} 1 \\ 0, \frac{1}{2}, m \end{smallmatrix}\right) \mathrm{d}u. \tag{49}$$

Integral in (49) is solved with the help of [26, (07.34.21.0013.01)], and derived final closed-form expression for the threshold-based error probability is given in (21).

REFERENCES

[1] U. Raza, P. Kulkarni, and M. Sooriyabandara, "Low power wide area networks: an overview," *IEEE Commun. Surv. Tutor.,* vol. 19, no. 2, pp. 855-873, Secondquarter 2017.

[2] A. Laya, L. Alonso, and J. Alonso-Zarate, "Is the random access channel of LTE and LTE-A suitable for M2M communications? A survey of alternatives," *IEEE Commun. Surv. Tutor.*, vol. 16, no. 1, pp. 4-16, First Quarter 2014.

[3] G. Durisi, T. Koch, and P. Popovski, "Toward massive, ultrareliable, and low-latency wireless communication with short packets," *Proc. IEEE*, vol. 104, no. 9, pp. 1711-1726, Sept. 2016.

[4] M. Haenggi and R. K. Ganti, "Interference in large wireless networks," *Found. Trends Netw.*, vol. 3, no. 2, pp. 127-248, 2009.

[5] M. Haenggi, "Stochastic geometry for wireless networks," *Cambridge University Press*, 2012.

[6] F. Baccelli, B. Blaszczyszyn, and P. Muhlethaler, "An Aloha protocol for multihop mobile wireless networks," *IEEE Trans. Inf. Theory*, vol. 52, no. 2, pp. 421-436, Feb. 2006.

[7] Y. Polyanskiy, V. H. Poor, and S. Verdú, "Channel coding rate in the finite blocklength regime," *IEEE Trans. Inf. Theory*, vol. 56, no. 5, pp. 2307–2359, 2010.

[8] G. Durisi, T. Koch, J. Oestman, J. Polyanskiy, and W. Yang, "Short-packet communications over multiple-antenna Rayleigh-fading channels", *IEEE Trans. Inf. Theory*, vol. 56, no. 5, pp. 2307-2359, May 2010.

[9] T. D. Novlan, H. S. Dhillon, and J. G. Andrews, "Analytical modeling of uplink cellular networks," *IEEE Trans. Wirel. Commun,* vol. 12, no. 6, pp. 2669-2679, June 2013.

[10] Q. Song, X. Lagrange, and L. Nuaymi, "Evaluation of macro diversity gain in long range ALOHA networks," *IEEE Commun. Lett.*, vol. 21, no. 11, pp. 2472-2475, Nov. 2017.

[11] R. Vaze, "Random Wireless Networks: An Information Theoretic Perspective," *Cambridge University Press*, 2015.

[12] N. Hesham and A. Chaaban, "On the performance of large-scale wireless networks in the finite block-length regime," in *Proc. IEEE ICC*, Montreal, QC, Canada, pp. 1-6, 2021.

[13] N. Hesham, J. Hossain, and A. Chaaban, "Transmission rate analysis for large scale uplink networks in the finite block-length regime," in *Proc. IEEE WCNC* 2023, Glasgow, United Kingdom, pp. 1-6, 2023.

[14] S. Tao, Y. Wang, C. Wang, J. Wang, and Y. Duan, "Meta Distribution Analysis in Finite Blocklength Communications," *IEEE Trans. Veh. Technol.*, early access, 2023.

[15] I. Ramezanipour, P. Nouri, H. Alves, P. H. Nardelli, R. D. Souza and A. Pouttu, "Finite blocklength communications in smart grids for dynamic spectrum access and locally licensed scenarios," *IEEE Sens. J.*, vol. 18, no. 13, pp. 5610-5621, 2018.

[16] R. Ma, W. Yang, X. Guan, X. Lu, Y. Song and D. Chen, "Covert mmWave communications with finite blocklength against spatially random wardens," *IEEE Internet Things J.*, early access, 2023.

[17] K. Singh, S. K. Singh, C. P. Li, "On the performance analysis of RIS-assisted infinite and finite blocklength communication in presence of an eavesdropper", *IEEE OJ-COMS,* 4, pp. 854-872, 2023.

[18] J. Park, J. P. Hong, W. Shin and S. Kim, "Performance analysis of distributed antenna system for downlink ultrareliable low-latency communications," *IEEE Syst J.*, vol. 15, no. 1, pp.518-525, 2020.

[19] H. Ji, S. Park and B. Shim, "Sparse Vector Coding for Ultra Reliable and Low Latency Communications," *IEEE Trans. Wirel. Commun.*, vol. 17, no. 10, pp. 6693-6706, Oct. 2018.

[20] S. Xing, X. Xu, Y. Chen, Y. Wang and L. Zhang, "Advanced Grant-Free Transmission for Small Packets URLLC Services," *2019 IEEE ICC Workshops*, Shanghai, China , pp. 1-5, 2019.

[21] M. Simon and M. Alouni "Digital communication over fading channels," *Wiley 2nd ed.*, New York, USA, 2004.

[22] H. A. Ammar, Y. Nasser, and H. Artail, "Closed form expressions for the probability density function of the interference power in PPP networks," in *Proc. IEEE ICC*, Kansas City, MO, USA, pp. 1-6, 2018.

[23] R. S. Anderssen, S. A. Husain, and R. J. Loy, "The Kohlrausch function: properties and applications," *Anziam J.*, vol. 45, pp.800–816, 2004.

[24] I. Gradshteyn and I. Ryzhik, *Table of integrals, series, and products*, 5th ed. San Diego, CA, USA: Academic, 1994.

[25] B. Makki, T. Svensson, and M. Zorzi, "Finite block-length analysis of spectrum sharing networks: interference-constrained scenario," *IEEE Wirel. Commun.*, vol. 4, no.4, pp. 433-436, 2015.

[26] The Wolfarm Functions Site, 2008. [Online]. Available: http:/functions.wolfarm.com